Materials Chemistry and Physics 313 (2024) 128671

Contents lists available at ScienceDirect

Materials Chemistry and Physics

journal homepage: www.elsevier.com/locate/matchemphys

Detection of Fe(III) ion based on bifunctionalized silver nanoparticles: Sensitivity, selectivity and environmental safety

Arianna Bellingeri [a,1], Federica Bertelà [b,1], Luca Burratti [b,1], Andrea Calantropio [a], Chiara Battocchio [b], Pietro Lupetti [c], Eugenio Paccagnini [c], Giovanna Iucci [b], Martina Marsotto [b], Paolo Prosposito [d], Ilaria Corsi [a], Iole Venditti [b,*]

[a] Department of Physical, Earth and Environmental Sciences, University of Siena, Via Mattioli 4, Siena, 53100, Italy
[b] Sciences Department, Roma Tre University, Via della Vasca Navale 79, 00146, Rome, Italy
[c] Department of Life Sciences, University of Siena, Via Aldo Moro, 2, 53100, Siena, Italy
[d] Department of Industrial Engineering, University of Rome Tor Vergata, Via del Politecnico 1, Rome, 00133, Italy

HIGHLIGHTS

- AgNPs are synthetised with two capping agents, citrate and glutathione.
- The size and stability control in water (Ø = 4 ± 0.2 nm; ζ-potential = - 60 ± 1 mV) was performed.
- The selectively detection of Fe (III) in the range 0.5–10.0 ppm was verified.
- The environmental safety assessment was evaluated with freshwater and marine microalgae.

ARTICLE INFO

Keywords:
Silver nanoparticles
Plasmonic sensors
Fe(III) detection
Glutathione
Ecosafety

ABSTRACT

Functionalized silver nanoparticles (AgNPs) are widely used as optical sensors for heavy metal ions in water, due to their versatile, easy and cheap preparations and due to their peculiar physico-chemical properties. Surface functionalization plays a key role in AgNPs chemical-physical behavior as capping agents can affect sensitivity, selectivity but alsoenvironmental safety. In this framework, AgNPs are synthetised and properly functionalized using two capping agents to induce hydrophilic behavior and selectivity, respectively citrate (cit) and glutathione (GSH). The opportune choice of these capping agents induces size control and stability for AgNPs-cit-GSH in water (Ø = 4 ± 0.2 nm; ζ-potential = - 60 ± 1 mV) and make available selectively detection of Fe (III) in the range 0.5–10.0 ppm. Environmental safety was also evaluated using standardized ecotoxicity assays (ecosafety) with freshwater and marine microalgae which show a low-to-negligible effects, with exception only at the highest tested concentration (10 mg/L) but only for the freshwater one.

1. Introduction

Metallic elements play a key role in several industrial fields, such as in optoelectronics, energy and catalysis, but they are also essential components of living beings [1–6]. Suffice it to say that metal ions are present in vitamins, coordinate with nucleic acids and hormones and play a decisive role in the modulation and regulation of biochemical processes [7–9]. However, an excessive or insufficient amount of some metal ions leads to an imbalance of metabolism and thus to disease. Therefore, quantitative determination of metal ion concentration is key to ensuring that metal ions are at a healthy level and not causing any harm to living beings [10]. Among others, Fe(III) is an essential element being involved in many physiological processes (i.e., transfer and transport of oxygen and block materials in either plants and animals

* Corresponding author.
E-mail addresses: arianna.bellingeri2@unisi.it (A. Bellingeri), federica.bertela@uniroma3.it (F. Bertelà), luca.burratti@uniroma3.it (L. Burratti), andrea.calantropio@student.unisi.it (A. Calantropio), chiara.battocchio@uniroma3.it (C. Battocchio), pietro.lupetti@unisi.it (P. Lupetti), eugenio.paccagnini@unisi.it (E. Paccagnini), giovanna.iucci@uniroma3.it (G. Iucci), martina.marsotto@uniroma3.it (M. Marsotto), paolo.prosposito@uniroma2.it (P. Prosposito), ilaria.corsi@unisi.it (I. Corsi), iole.venditti@uniroma3.it (I. Venditti).
[1] these authors contributed equally.

https://doi.org/10.1016/j.matchemphys.2023.128671
Received 10 August 2023; Received in revised form 26 October 2023; Accepted 10 November 2023
Available online 2 December 2023

including humans [11]. The lack of Fe ions will result in many disruption of physiological function and cause of pathological diseases, such as iron-deficiency anaemia, methemoglobinemia, liver and kidney damage, diabetes and heart diseases, and so on. Iron overload is frequently found in transfused patients with chronic anemia and congenital hemochromatosis. Iron toxicity adversely affects organs, including the heart, liver, and endocrine glands [12]. Iron is the second most abundant element in the earth crust and plays critical roles in many natural processes such as biogeochemical cycles and plant metabolism, while is also a growth-limiting factor in marine ecosystems [13,14]. Iron is typically present in acid mine drainage (AMD), which is produced when sulfide-bearing material is exposed to oxygen and water. All these reasons make of significant importance to develop accurate and simple tools for the quantitative determination of Fe in complex matrices either environmental ones and/or pharmaceuticals, or industrial [15]. Several studies have been carried out on the sensitive and selective detection of Fe(III) ions [16,17]. Ghosh et al. synthesized two fluorescent 1-naphthylamine derivatives and found that both are selective and sensitive toward Fe(III) ions [18]. Li et al. showed that an L-cysteine capped Fe3O4@ZnO core−shell nanoprobe can selectively detect Fe(III) ion in both serum and wastewater samples [19]. In the context of nanoscale sensors, silver nanoparticles (AgNPs) have received increasing attention in colorimetric assay because of their pronounced surface plasmon resonance (SPR), highly stable dispersion, easy chemical functionalization and tunable chemo-physical properties [20–22].

In this context, bifunctionalized and click-synthesized AgNPs are of great interest because the two functionalizations can have a cooperative effect on pollutant recognition, resulting in appreciable changes in color and adsorption properties. This makes the system more efficient in terms of selectivity and sensitivity. In many works in the environmental field, bifunctionalized AgNPs have highlighted the role of two ligands: generally, one of the two allows good stability in the medium of use, and this improves the possibility of interaction with the pollutant, and the second creates a more specific and selective interaction1) [23–25].

Furthermore, in the last decade numerous studies have been started to obtain AgNPs that are sustainable from an environmental point of view and also safe by design [26–28]. Nevertheless, to the best of our knowledge, the selective and sensitive detection of Fe(III) based on bifunctionalized AgNPs has not yet been performed.

Herein, the synthesis of AgNPs functionalized by citrate (cit) and glutathione (GSH) was achieved in order to obtain a selective and sensitive sensor for Fe(III), through SPR variations. This pair of capping agents is chosen to obtain a high hydrophilicity of the system thanks to cyt and a specific interaction of GSH with Fe(III). Furthermore, this choice allows for a synthesis in the aqueous phase that is easy, economical and free of solvents or polluting acid reagents. Structural characterizations were performed and the sensing mechanism based on Fe (III) interaction with functionalized nanoparticles surface was proposed. Moreover, in order to speed their environmental application along with their safety, an environmental safety assessment (ecosafety) was performed by using ecotoxicity assays on two primary producers, the freshwater microalga *Raphidocelis subcapitata* and the marine microalgae *Dunaliella tertiolecta,* was done.

2. Experimental section

2.1. Materials

Reagents and solvents of analytical grade were purchased from Sigma-Aldrich (St. Louis, MO) and were used without further purification. Silver nitrate ($AgNO_3$, 99.9% pure), sodium citrate ($Na_3C_6H_5O_7$, 99% pure), L-Glutathione reduced ($C_{10}H_{17}N_3O_6S$, 98% pure), sodium borohydride ($NaBH_4$, 99.9% pure), sodium hydroxyde (NaOH, 98%) and nitric acid (HNO_3, 70%). Table S1 in Supplementary Material shows the list of the 15 metal ions employed for selectivity tests. All reagents were purchased from Merck (Darmstadt, Germany) without further purification processes and dissolved in deionized water (18.2 MΩ cm).

R. subcapitata (freshwater microalga) was obtained from the Italian Institute for Environmental Protection and Research (ISPRA) and cultured in TG201 medium (OECD 201). *D. tertiolecta* (marine microalga) was obtained from the Regional Agency for Environmental Protection of Tuscany (ARPAT) and cultured in F/2 medium (ISO 2006:10253).

2.2. Synthesis of AgNPs-cit-GSH

The AgNPs-cit-GSH were synthetised in analogy with our previous works [29,30]. Chemical synthesis in brief: water solutions of GSH (0.002 M, 5 mL), cit (0.01 M, 200 mL) and $AgNO_3$ (0.05 M, 5 mL) were added in glass flask. The resulting solution was mixed and degassed with Argon for 5 min, then a water solution of $NaBH_4$ (0.016 g in 4 mL) was added to the mixture. After 2 h the dark yellow suspension was collected and purified by centrifugation (13000 rpm for 30 min).

2.3. Characterization

The obtained AgNPs-cit-GSH suspensions were characterized by means of UV–Vis, using quartz cells with a Shimadzu 2401 UV–vis spectrophotometer, and Dynamic Light Scattering (DLS), with the Zetasizer Nano ZS90 (Malvern) combined with the Zetasizer Nano Series software (version 7.02, Particular Sciences) [31–33]. DLS measurements were performed at a concentration of 50 mg/L in milliQ water at 25 °C. Before each withdrawal or dilution from the purified reaction lot, the AgNPs-cit-GSH suspensions was sonicated in an ultrasonic bath (Mod. CP316, Ceia) for 10 s. Transmission electron microscopy (TEM) images were obtained by means of a Tecnai G2 Spirit (FEI) on 50 mg/L sample of AgNPs-cit-GSH in milliQ water. For a further analysis of the particle size, the diameter of the totality of the particles (29) counted in 4 TEM images was measured with imageJ software. Fourier Transform Infrared FT-IR measurements were performed by means of a VECTOR 22 (Bruker) FT-IR interferometer equipped with a DTGS detector operating in the wavenumber range 400–4000 cm^{-1}, with a resolution of 1 cm^{-1}. Pristine GSH was analyzed in transmittance mode as pressed KBr pellets. Reflection-Absorption InfraRed Spectroscopy (RAIRS) measurements were performed on thin films of AgNPs-cit-GSH deposited on a reflecting gold substrate with a Specac P/N 19650 series monolayer/grazing angle accessory; spectra were recorded at incidence angles of 70° with respect to the normal to the sample surface.

2.4. Advanced Spectroscopic characterizations

X-ray Photoelectron Spectroscopy (XPS) analysis on AgNPs-cit-GSH and AgNPs-cit-GSH + *Fe(III)* samples (realized from interaction with Fe(III) at 5.0 ppm) was performed with a homemade instrument, consisting of preparation and analysis Ultra High Vacuum (UHV) chambers separated by a gate valve. The analysis chamber is equipped with a six-degree-of freedom manipulator and a 150 mm mean radius hemispherical electron analyzer with a five-lens output system combined with a 16-channel detector giving a total instrument resolution of 1.0 eV as measured at the Ag $3d_{5/2}$ core level. Samples were introduced in the preparation chamber and left outgassing overnight at a base pressure of about 10^{-8} Torr, before introduction in the analysis chamber. Typical vacuum pressure in the analysis chamber during measurements was in the 10^{-8}–10^{-9} Torr range. The used X-ray radiation is a non-monochromatized MgKα (1253.6 eV). Calibration of the energy scale was made referencing the spectra to the C1s core level signal of aliphatic C atoms, found at 285.0 eV, for all samples [34]. Atomic ratios were calculated from peak intensities using Scofield's cross-section values [35]. Curve-fitting analysis of the C1s, N1s, O1s, S2p, Ag3d and Fe2p spectra was performed using Gaussian profiles as fitting functions, after subtraction of a polynomial background. The $S2p_{3/2}$-$S2p_{1/2}$, $Ag3d_{5/2,3/2}$ and $Fe2p_{3/2,1/2}$ doublets were fitted using the same full width at half

maximum (FWHM) for the two spin-orbit components of the same signal, a spin-orbit splitting of 1.20 eV for S2p, 6.00 eV for Ag3d, 13.20 eV for Fe2p, and the branching ratios $S2p_{3/2}/S2p_{1/2} = 2$, $Ag3d_{5/2}/Ag3d_{3/2} = 3/2$, $Fe2p_{3/2}/Fe2p_{1/2} = 2$, respectively.

High Resolution XPS (HR-XPS) experiments were carried out at the PM4 beamline at the BESSYII synchrotron facility in Berlin (DE), using the end-station Low Dose PES equipped with a Scienta ArTOF-2 electron energy analyzer [36]. For the C1s, O1s, N1s, Ag3d spectral regions, photon energy of 600 eV was used; for the S2p spectral region, a photon energy of 360 eV was selected, as to maximize signal intensity. For measuring Fe2p core level, a photon energy of 1000 eV was selected. The energy resolution was $\Delta E = 0.44$ eV across the entire energy range. Calibration of the energy scale was made referencing the spectra to the C1s core level signal of aliphatic carbons, positioned at 285.00 eV coherently with literature [34]. Curve-fitting analysis of the C1s, O1s, S2p, Ag3d, $Fe2p_{3/2}$ spectra was done using Gaussian curves as fitting functions, after subtracting a polynomial background. The $S2p_{3/2,1/2}$ doublets were fitted using the same FWHM for both components, a spin−orbit splitting of 1.2 eV, and a branching ratio ($2p_{3/2}/2p_{1/2}$) of 2. For the $Ag3d_{5/2,3/2}$ doublets, a splitting of 6.0 eV, a branch ratio $3d_{5/2}/3d_{3/2}$ of 3/2 and the same FWHM values for both spin−orbit components were applied. When several different species were identified in a spectrum, the same FWHM value was set for all individual photoemission bands.

2.5. Optimization of the optical sensor

The parameters such as interaction time, AgNPs-cit-GSH concentration and pH were optimized to obtain the best condisions for the optical response. The Fe(III) concentratration of 5.0 ppm was selected as quantity probe for the optimization processes.

Three different AgNPs-cit-GSH concentrations were studied: 2 mg/mL, 1 mg/mL and 0.5 mg/mL; first the spectra were recorded without Fe (III) and after, the measurements were repeted once polluted the samples, finding that the best option is 0.5 mg/mL.

The optical response of AgNPs-cit-GSH at the pH values of 2, 4, 6, 8, 10 and 12 was studied to ensure the stability of the colloidal solution. Buffer solutions at those pH values were prepared by using HNO_3 and NaOH, both at the concentration of 1 M. Once stability has been ascertained, the solutions were polluted by adding Fe(III) solution to reach the final concentration of 5 ppm, the absorption spectra were recorded again.

2.6. Selectivity and sensitivity tests

The selectivity of AgNPs-cit-GSH was studied with the metal ions listed in Table S1. A UV–vis spectrophotometer (Lambda 750, PerkinElmer) served for measuring the SPR peak of AgNPs colloidal solution in the wavelength range 300–700 nm. Disposable plastic cuvettes with an optical path equal to 10 mm was employed during the measurements. The absorption spectrum of AgNPs-cit-GSH solution was recorded before the interaction with metal ions (M^{n+}) as reference, and after 5 min of incubation with the M^{n+} at the concentration of 5.0 ppm. The results shown in the 3.2 section, underline an exclusive selectivity for Fe(III). The same procedure was applied to the sensitivity tests where the Fe(III) concentration was changed as follows: 0.5, 1.0, 2.5, 5.0, 7.5 and 10.0 ppm.

2.7. Ecosafety assessment

AgNPs-cit-GSH batch was tested on primary producers through a standardized microalgal growth inhibition assay (OECD 201 2011, ISO/10253 2006) using the freshwater microalga *R. subcapitata* and the marine microalga *D. tertiolecta* Microalgae were cultured in TG201 medium (*R. subcapitata*) in MilliQ water and F/2 medium (*P. tricornutum*) in filtered (0.45 μm) natural seawater (NSW) and maintained in axenic exponential growth conditions at 18 ± 1 °C with a 16/8 h light-dark cycle photoperiod in a growth chamber. Microalgae were pre-cultured for 72 h at 21 ± 1 °C and continuous illumination at 4500 lux, to ensure exponential growth. Assays were carried out in 24-multi-well plates with an initial algal concentration of 1×10^4 cells/mL and exposed as follows: 0 (CTRL), 0.001, 0.01, 0.1, 1, 10 mg/L for AgNPs-cit-GSH and 0.001, 0.01, 0.1, 0.5, 1 mg Ag/L for $AgNO_3$, used as a reference toxicant. Three replicates for each exposure concentration were set. After 72 h, algae were fixed with a 1:1 (v/v) Lugol/ethanol solution, and cell number was determined utilizing an automated cell counter (LUNA II, Logos Biosystems). Microalgae concentration (cells/mL), growth rate (μ), and growth inhibition (Iμi) *vs* controls (only in medium) were determined.

3. Result and discussion

3.1. Synthesis of AgNPs-cit-GSH

In the synthesis of AgNPs, the choice of the binder plays a key role and many recent works show how, as the capping agent varies, the properties of the particle itself can be modulated [37,38].

Initially, AgNPs-cit, with only citrate (cit), and AgNPs-GSH, with only glutathione (GSH) were prepared in our laboratory. However, AgNPs-cit showed no significant sensitivity and selectivity, while AgNPs-GSH were obtained in rough shape and size, like small pebbles, without plasmon. This did not surprise us, because, unlike many literature articles in which the synthesis of these nanoparticles is presented, in our laboratory we chose to study the synthesis without the use of polluting solvents, therefore also avoiding acids and bases, for also limit the possible environmental impact in the production of nanoparticles. For these reasons, in our case, it was decided to introduce a double surface functionalization using two ligands, cyt and GSH, capable of guaranteeing both high hydrophilicity/stability in water and good biocompatibility [29,39]. The synthesis takes place in a single step in water at room temperature, using sodium borohydride as a reducing agent. Fig. 1a) depicts the absorption spectrum of a water suspension of freshly prepared AgNPs-cit-GSH, showing the SPR peak at $\lambda_{max} = 370$ nm and full width at half maximum (FWHM) equal to 170 nm. The position of the peak and the shape of the band are related to the size and polydispersity of the particles [40]. After the synthesis, unbound cit and GSH molecules are present in the reaction mixture and high-speed centrifugation is used to remove them: the unreacted molecules, as well as the secondary products of sodium borohydride, remain in the supernatant which is then separated from the precipitated particles. In particular, we can hypothesize that GSH binds covalently to the metal surface via S and this, together with the presence of citrate, stabilizes the nanoparticles. The nanoparticles are quite stable at room temperature up to 9 months as demonstrated by the UV–vis spectra recorded in different time intervals (Fig. S1 in Supplementary Material). Since the use of these particles is foreseen in water, it was fundamental to study the hydrodynamic dimensions and the ζ-potential of the nanoparticle by DLS, as reported in Table 1 and Fig. 1 b,c).

The $<2R_H>= 60.8 \pm 0.2$ nm shows a dimension less than 100 nm which can easily interact at a biological level with plants and microorganisms. The ζ potential = - 60.8 ± 0.2 mV shows a negative charge due to both the presence of the citrate and the GSH with deprotonated COOH acid group: an excellent situation both for keeping the particles stable and for being able to interact with any heavy metal ions in the water. Furthermore, TEM investigations were carried out which confirmed the size and spherical shape of the particles with average diameter 11 ± 4 nm, as shown in Fig. 1 d).

3.2. Optimizzation processes of the sensor

The sensor responsivity was optimized by changing parameters such as the AgNPs-cit-GSH concentration and pH. Fig. S2 (a) shows the UV–Vis absorption specta as a function of AgNPs-cit-GSH

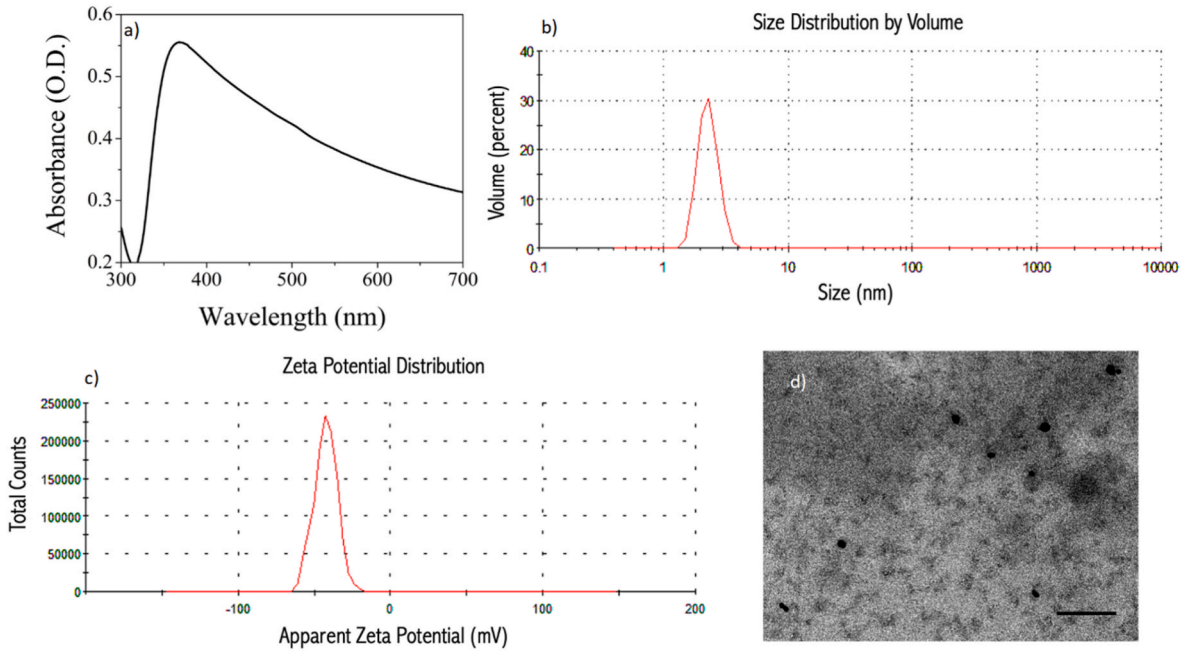

Fig. 1. Main characterizations of AgNPs-cit-GSH: **a**) Uv–vis spectrum in water: $\lambda_{max} = 370$ nm; **b**) Size distribution by Volume as measured by DLS in MilliQ water at 25 °C; **c**) ζ potential - 60.8 ± 0.6 mV in MilliQ water at 25 °C; d) TEM image of AgNPs-cit-GSH (scale bar = 100 nm).

Table 1
Main AgNPs-cit-GSH features: UV–Vis peak ($\lambda_{max} = 370$ nm), average diameter as measured by TEM (nm), $<2R_H>$ by DLS, Polidispersity Index (PDI) and ζ -potential, in MilliQ water.

λ_{max} (nm)	Average diameter by TEM (nm)	$<2R_H>$ by Intensity (nm)	$<2R_H>$ by Volume (nm)	PDI	ζ-potential (mV)
370	11 ± 4	60 ± 0.2	4 ± 0.4	0.5	−60 ± 0.6

concentrations: 2 mg/mL, 1 mg/mL and 0.5 mg/mL. For the case of 2 mg/mL the concentration is too high for the instrument, in fact, this concentration produces the saturation of the spectrophotometer and this concentration can not be used for sensing purpose. On the countrary, concentrations below 0.5 mg/mL would be difficult to measure. Subsequently, the samples at 1 mg/mL and 0.5 mg/mL were were tested in presence of Fe(III) and the ratio $(I - I_0)/I_0$ was calculated, where, I and I_0 represent the absorbance values of the SPR band at 370 nm (maximum) for polluted and pristine AgNPs-cit-GSH solutions, respectively, obtaineing that the highest response were found for 0.5 mg/mL, as reported in Fig. S2 (b). For these reasons, the 0.5 mg/mL concentration was selected for all the measurements.

The stability of AgNPs-cit-GSH at different pH was also investigated. Fig. S3 (a) shows the optical absorption of AgNPs-cit-GSH at different pH values (from 2 to 12), where except for the sample at pH = 2, the others remained stable in the wide range from 4 to 12, testifying that the choice to use 2 different capping agents was successful. For the pH value of 2, the plasmon band decreases conspicuously, and in addition after few hours the typical color of the colloidal solution turned to transparent and colorless. Once studied the stability, the optical response to Fe(III) at the different pH values was explored. By calculating the ratio $(I - I_0)/ I_0$ [see Fig. S3 (b) of the Supplementary Material)]we obtained that the negative response for sample at pH 2 is due to the instability of AgNPs and not to the presence of Fe(III), while the optical response is almost the same for the range between 4 and 8, but it slightly increases for vary basic conditions. We concluded that for high acidity of the medium, the capping agents (GSH and citrate) will be completely protonated, the electrostatic shield decreases with subsequent destabilization of the nanoparticles. Glutathione and citric acid have acid dissociation constants equal to 2.1, 3.6, 8.8, 9.7 and 3.1, 4.8, 6.4, respectively [41, 42]. For values within 4–8, the protonation of capping agents is partial and the interaction with Fe(III) is almost constant, while for very basic conditions, the protonation for both capping agents is absent and the interaction between Fe(III) and AgNPs is stronger as well as the optical response. We decided to fix the pH value to 6 for all the remaining characterizations, as this value is closer to the conditions of real samples.

3.3. Detection of Fe(III)

Fig. 2 a shows the optical absorption spectra of pristine AgNPs-cit-GSH colloidal solution and those contaminated by different concentrations of Fe(III) (from 0.5 to 10.0 ppm). In presence of Fe(III) ions, the peak position does not change, meanwhile the FWHM undergoes a narrowing of about 120 nm (for the10.0 ppm sample). The most striking change in the SPR is certainly the increase in the background, which moves the band up, testifying the occurred interaction between Fe(III) ions and the AgNPs. By plotting, the dimensionless ratio between the ratio $(I-I_0)/I_0$, it has been possible to obtain a linear graph as reported in Fig. 2 b and to calculate the limit of detection (LOD, 3σ) of this system, that is equal to 0.7 ppm. Fig. 2 c represents the selectivity tests, measuring the optical absorption of AgNPs-cit-GSH colloidal solution before and after contamination of M^{n+}. The ratio $(I - I_0)/I_0$ highlights the strong optical response of AgNPs-cit-GSH towards Fe ions, indeed, the other 14 metal ions do not affect the SPR band of AgNPs-cit-GSH, in terms of peak position, bandwidth neither intensity, as reported in Fig. S4 in Supplementary Material. To evaluate the interference of different anionic species, the experimental procedure was repeated using tap water specially polluted with Fe(III) (from 0.5 to 10.0 ppm), the results are showed in Fig. 2 d. The optical response remained unchanged even with the co-presence of different ions (see Table S2 of the Supplementery Material for the chemical composition of the tap water), reporting a sensitivity and linearity comparable to that in deionized water (Fig. S5 of the Supplemantary Material). Finally, the sensitivity test against Fe(III) was repeated after 130 days from the date of the AgNPs synthesis, to evaluate the reliability of the sensing performance. The results are showed in Fig. S6 and almost the same results were obtained in terms of optical response.

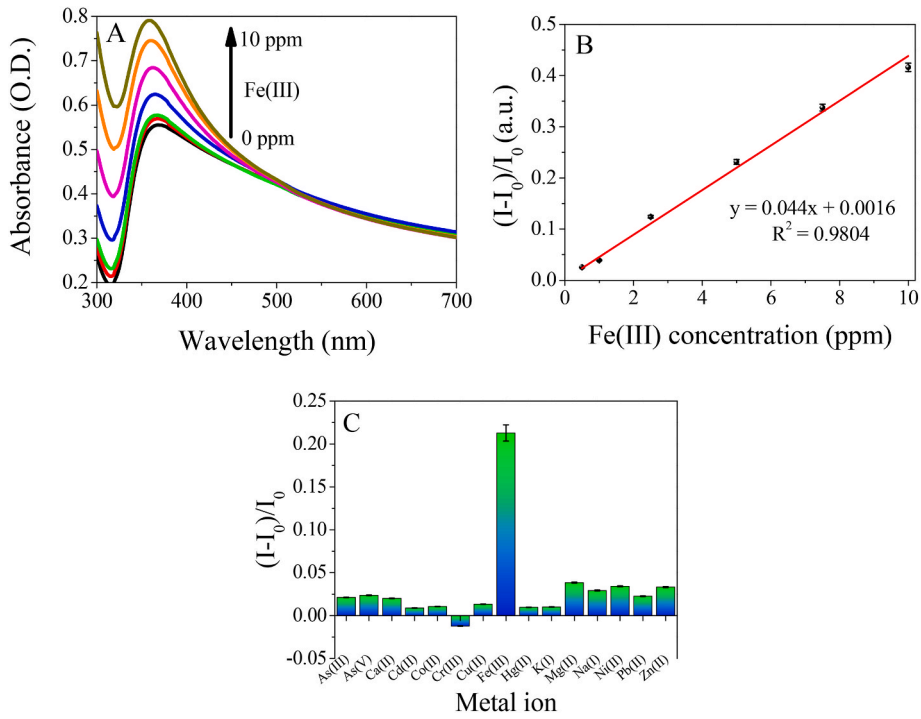

Fig. 2. **a**) UV–Vis spectroscopy of AgNPs-cit-GSH colloidal solution before (black curve) and after interaction with different concentrations of Fe(III); **b**) dimensionless ratio $(I - I_0)/I_0$ a function of Fe(III) ions concentration, the red line represents the best fit of experimental points; **c**) selectivity tests with 15 different metal ions at the concentration of 5.0 ppm; **d**) UV–Vis spectroscopy of AgNPs-cit-GSH colloidal solution before (black curve) and after interaction with different concentrations of Fe(III) in tap water.. (For interpretation of the references to color in this figure legend, the reader is referred to the Web version of this article.)

Table 2 shows various systems designed for the detection of Fe3+. It can be seen that the present nanomaterial exhibits a lower LOD than most reported systems: the good sensitivity of the system can be deduced, in addition to the selectivity already shown. Furthermore, the simplicity of synthesis and cost-effectiveness make the AgNPs-cit-GSH very attractive sensing material.

3.4. Structural investigation of AgNPs-cit-GSH before and after exposure to Fe(III) ions

3.4.1. XPS and HR-XPS study

X-ray photoelectron spectroscopy measurements allowed to probe the interaction between AgNPs and Fe(III) ions. Spectra were collected at C1s, N1s, O1s, Ag3d, S2p and Fe2p core levels [all Binding Energy – BE (eV), FWHM (eV), atomic percentages and proposed signals assignments are reported in Supplementary Material file, Table S3]. All the individuated spectral components confirm AgNPs stability, and cit and GSH capping efficiency. In C1s spectra (Fig. 3) the components at 285.0, 286.6 and 288.4 eV BE, respectively associated with aliphatic carbons, C-S and C-N bond and N-C═O bond, confirm the presence of GSH on AgNPs surface [48]. Components at higher BE are in agreement with the presence of citrate and GSH. Comparing C1s spectra of AgNPs-cit-GSH before and after interaction with Fe(III), there are no significant differences; this suggests that the capping agents molecular structure is unattained by the treatment.

Table 2
Performance of different sensors for Fe (III) detection.

Detection system	Linear Range	Detection Limit	Ref.
Gold nanoparticles	0-100 (μM)	5.6 (μM)	[43]
GQD: Graphene Quantum Dots	0-400 (μM)	7.2 (μM)	[44]
MOF: metal organic framework	3-200 (μM)	9 (μM)	[45]
PPE-containing, fluorescent polydimethylsiloxane (PDMS) pad.	0–0.5 (mM)	2 ppm	[46]
AgNPs-N-acetyl-l-cysteine	0.08–80 (μM)	80 (nM)	[47]
AgNPs-cit-GSH	0–10 ppm 0–50 μM	0.7 ppm 3.5 μM	This work

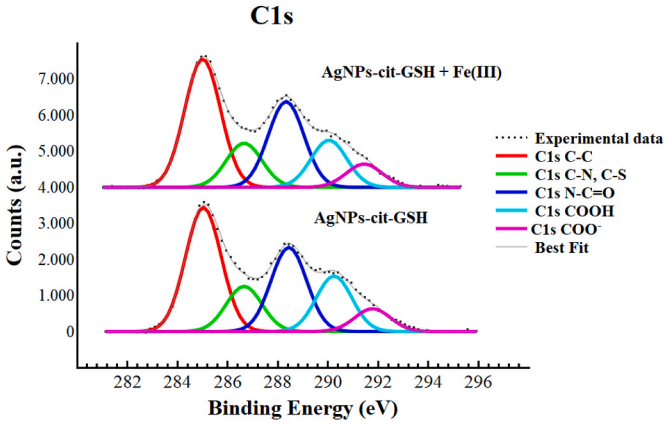

Fig. 3. XPS spectra collected on AgNPs-cit-GSH and AgNPs-cit-GSH + Fe(III) at C1s core level.

To obtain spectra with improved resolution, allowing to observe modifications in the signals shape and position induced by the nanoparticles interaction with iron ions, N1s, S2p and Fe2p core levels signals were also collected by synchrotron radiation-induced X-ray photoelectron spectroscopy (HR-XPS). Complete HR-XPS data analysis results [BE (eV), FWHM (eV), Atomic percentages and proposed assignments for all measured signals components] are reported in Supplementary Material file, Table S4. N1s spectra of AgNPs-cit-GSH before and after exposure to Fe(III) (Fig. 4 a, d) show two components at 398.6 and 399.9 eV BE, respectively associated with R-NH_2 and NHCO; the spectral components individuated in the two N1s spectra have the same BE and very similar intensity ratios, suggesting that the N-containing functional groups are

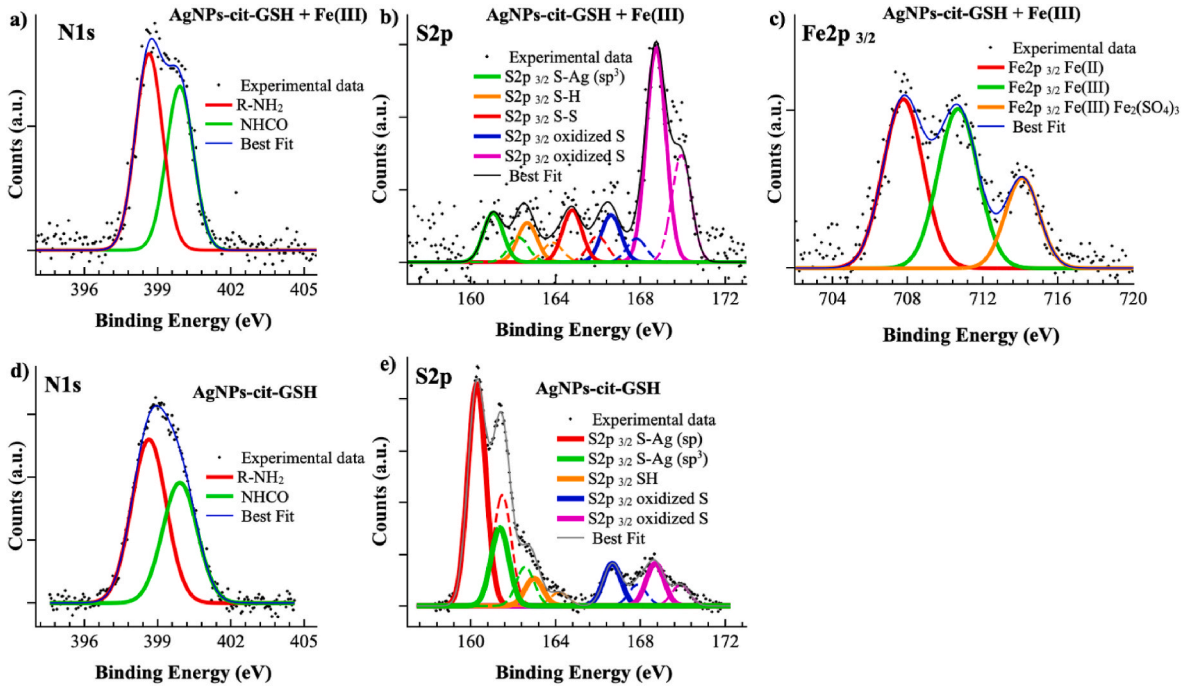

Fig. 4. SR-XPS spectra collected on AgNPs-cit-GSH + Fe(III) at (**a**)N1s, (**b**) S2p and (**c**) Fe2p (high-resolution acquisition of the Fe2p $_{3/2}$ spin-orbit component) core levels, and SR-XPS spectra collected on AgNPs-cit-GSH at (**d**)N1s and (**e**) S2p core levels.

not directly involved in the interaction with Fe(III). On the other hand, S2p spectra show some intensity variation subsequent to the interaction between AgNPs-cit-GSH and iron ions. As reported in Fig. 4 b and e, S2p spectra show several spin orbit pairs: the signals at lower BE ($S2p_{3/2}$ = 160.3 eV and $S2p_{3/2}$ = 161.4 eV in AgNPs-cit-GSH) are both indicative for sulphur atoms covalently bonded to silver, but with two different hybridizations, sp and sp^3 – hybridized S atoms [49]; in AgNPs-cit-GSH + Fe (III) 5 ppm only the component associated with sp^3 – hybridized S atoms is observed. At higher BE values it is possible to individuate features attributed to physisorbed thiol moieties ($S2p_{3/2}$ = 163.0 eV) and dithiol S-S groups ($S2p_{3/2}$ = 164.5 eV). At very high BE values (167–168 eV), at least two signals attributed to oxidized S are detected. Interestingly, the intensity of such features considerably increases in AgNPs-cit-GSH + Fe (III) 5 ppm, in good agreement with FT-IR findings (see next section).

To better understand the chemical interaction arising between AgNPs-cit-GSH and Fe(III) ions, Fe2p spectrum was also acquired at high resolution in the $Fe2p_{3/2}$ region. As shown in Fig. 4 c, it is possible to individuate at least three contributions to the $Fe2p_{3/2}$ feature, suggesting the presence of iron ions in different oxidation state and chemical environment. By comparison with the literature [38], the lower BE component ($Fe2p_{3/2}$ BE = 707.8) is associated to Fe(II) ions, while the two signals at higher BE are indicative for Fe(III) ions (710.7 eV) and Fe (III) ions in coordination compounds or iron sulphate $Fe_2(SO_4)_3$ (714.1 eV) [38], in excellent agreement with the presence of oxidized sulphur species pointed out in Fig. 4 b, as well as FT-IR observation of S═O groups in AgNPs-cit-GSH + Fe(III) spectra.

The high resolution-XPS data suggest that the interaction of iron ions with AgNPs-cit-GSH involve a redox process, with partial reduction of Fe (III) to Fe(II) and oxidation of -SH moieties of GSH to S-S (disulphides) but also to oxidized S-species, including sulphates; this finding is not surprising, since the oxo-reductive behavior of Fe(III) ions and glutathione, producing Fe(II) and dithiols (RS-SR) moieties, are widely discussed in the literature [50]. At the same time, HR-XPS spectra of Ag3d revealed an increased amount of Ag(I) with respect to the metallic silver (Fig. S7 in the Supplementary Materials); the atomic percent of Ag(I), arising by silver atoms at the NPs surface chemically interacting with thiol end groups is usually around 10–15% [51]; after interaction with Fe(III), the Ag(I) atomic percentage detected by HR-XPS is about 45% (see Table S4 in the Supplementary Material); this furtherly confirms the oxidative activity of Fe(III) ions, since oxidation of Ag atoms to Ag(I) in presence of ferric ions is also supported by the literature [52,53].

3.4.2. FTIR study

The FTIR spectra in the 4000-1000 cm^{-1} range of pristine glutathione (GSH), silver nanoparticles functionalized with glutathione (AgNPs-cit-GSH), and of the nanoparticles after interaction with Fe (III) (AgNPs-cit-GSH + Fe(III)) are shown in Fig. 5. The spectrum of glutathione is dominated by the C═O stretching vibration (labelled $\nu_{C═O}$ in the figure); the peak shows a complex structure, with contributions from different type of functions in the molecule (*i.e.,* amides and carboxyls); the main peak localized at 1600 cm^{-1} is mainly due C═O stretching of the amide function, possibly partially superimposed with the C═O stretching of the deprotonated carboxyls, while the shoulder at 1540 cm^{-1} is due to N-H bending vibrations (δ_{N-H}); the peak at 1710 cm^{-1} is related to protonated carboxyl functions ($\nu_{C═O\ pr}$). In the high frequency region, the two peaks at 3350 and 3250 cm^{-1} are related to the N-H stretching vibrations of the amine groups (ν_{N-H}), the peak at 3125 cm^{-1} to amide N-H stretching ($\nu_{N-H\ amd}$), peaks in the 3000-2800 cm^{-1} region are due to C-H stretching (ν_{C-H}) and the sharp peak at 2530 cm^{-1} originates from S-H stretching vibrations of the thiol group (ν_{S-H}). This later peak disappears in the spectrum of AgNPs-cit-GSH nanoparticles (spectrum b, red line), confirming that anchorage of the glutathione molecules to the AgNPs takes place through the thiol group. The C═O stretching vibration and other skeletal vibrations of glutathione (such as the peaks at 1390 and 1330 cm^{-1} labelled GSH in the figure) are still clearly visible in the spectrum of AgNPs-cit-GSH, though they appear slightly broadened, confirming the successful immobilization of glutathione on the nanoparticles surface. In the high frequency region, the broad band at 3350 cm^{-1} is related to the O-H stretching of physisorbed water, covering the N-H stretching of amines and amides. Interaction with Fe(III) cations (AgNPs-cit-GSH + Fe(III), spectrum c, blue line) does not produce significant changes in the IR spectrum, apart from a slight further broadening of all the peaks. The peak at 1120 cm^{-1} appears much broadened, with higher frequency contributions at about 1170 and 1250 cm^{-1} that could be related to the formation of S═O bonds ($\nu_{S═O}$). The peak at 2350 cm^{-1} is related to environmental CO_2 [54].

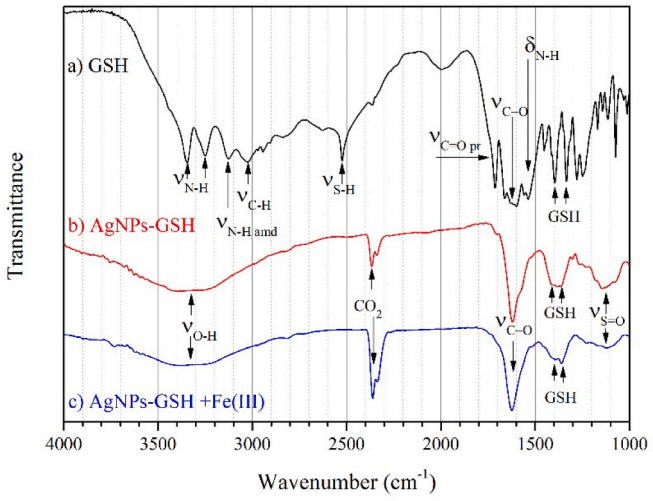

Fig. 5. FTIR spectra in the 4000-1000 cm^{-1} range of **a**) GSH, **b**) AgNPs-cit-GSH and **c**) AgNPs-cit-GSH + Fe (III).

3. 4.3. AgNPs-cit-GSH and Fe(III) interaction mechanism

The initial idea behind the development of these new silver nanoparticles was to achieve multiple functionality bonded on the metal surface. In fact, cyt manages to perform the dual role of hydrophilic capping agent, helping to modulate the presence of the second capping agent, *i.e.* GSH, so as to ensure the minimum quantity on the surface, capable in any case of responding to stimuli from the external environment, in particular in the presence of a few ppm of Fe(III). From the existing literature on the interaction of glutathione with Fe(III) it is evident the ability of the iron ion to oxidize glutathione, reducing itself [50]. This established fact together with the structural analyzes conducted lead to the definition of an interaction mechanism, as represented in Fig. 6, based on: i) the presence of a double layer of glutathione on the surface of the silver particles, a first layer chemisorbed, covalently bonded and the second physisorbed, due to hydrogen bonding interactions between amino and carboxyl groups of two different glutathione molecules: for the physisorbed layer it is easier to interact with the external environment; ii) in the presence of Fe(III) the physisorbed glutathione oxidizes forming disulphide bridges and more intense electrostatic interactions with Fe(II), separating the particles in a better way and causing an increase in the intensity of the plasmon peak which is even sharper. Furthermore, the silver surface is thus more exposed and Fe(III) can also oxidize it to Ag(I) releasing silver ions.

3.5. Ecosafety assessment

The ecosafety assessment of AgNPs-cit-GSH showed low ecotoxicity for both microalgae. In particular, the growth of the marine *D. tertiolecta* was not affected by any of the concentration tested, while the freshwater *R. subcapitata* showed a 50.5 ± 8 % inhibition of growth only at the highest concentration of 10 mg/L (Fig. 7 a). Conversely, reference toxicant $AgNO_3$ caused a marked toxicity on both microalgae, reaching a 100% inhibition for the freshwater *R. subcapitata* already at 0.1 mg Ag/L (Fig. 7 b).

AgNPs-cit-GSH are far less toxic for microalgae in comparison to other AgNPs batches having a different coating [55–58]. The protective role of sulphur groups toward ecotoxicity of AgNP has been reported previously and hypothesized to be linked to a reduced level of dissolution and release of free Ag ions, known to be partically responsible of ecotoxicity [59–61]. Moreover, the surface functionalization of AgNPs with biothiols, such as L-cysteine and glutathione, has been already demonstrated to be ecosafe by efficiently reduce AgNP ecotoxicity [29,30,62] as confirmed with the AgNPs-cit-GSH batch. Findings on $AgNO_3$ effect are in line with what reported in the literature, as Ag ions are known to be highly toxic to microalgae [63]. Also, the different outcome among freshwater and marine species was expected and can be explained by the different salinity of exposure media (0‰ for freshwater medium, 40‰ for marine medium) influencing Ag ions speciation reducing their bioavailability at high salinities [64,65].

4. Conclusion

In this work, the synthesis of AgNPs-cit-GSH functionalized by citrate (cit) and glutathione (GSH) was presented. This choice of pair of capping agents allows for high hydrophilicity of the system and selective interaction with Fe(III). Furthermore, the synthesis in the aqueous phase remains easy, cheap and free of polluting solvents or acid reagents. The particles nanodimension was confirmed by Uv–Vis spectrum (plasmonic peak at 370 nm), by TEM images (Ø = 11 ± 4 nm) and DLS studies ($<2R_H>$ = 4 ± 0.2 nm; ζ pot = - 60 ± 0.1 mV). AgNPs-cit-GSH evidenced selectivity and sensitivity for Fe (III) ion, in the range 0.5–10.0 ppm. The in-depth characterization of the system made possible to hypothesize a direct interaction between Fe(III) and GSH present on silver surface as capping agent, also responsible for high selectivity, compared to the 14 metal ions tested in water solution at 5.0 ppm. Moreover, the ecosafety assessment of AgNPs-cit-GSH batch confirm its suitability for a safer environmental application in terms of low-no impact for aquatic microalgae.

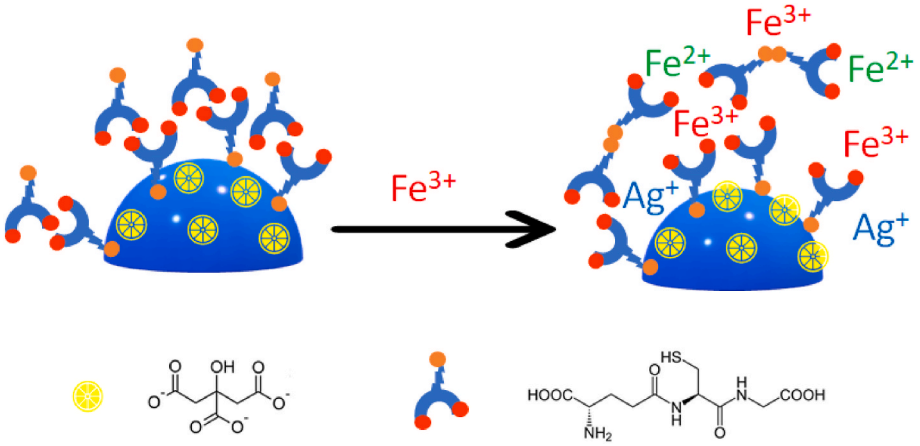

Fig. 6. Scheme of interaction between Fe(III) and AgNPs-cit-GSH: GSH bilayer on silver surface and disulphide bridges in presence of iron ions.

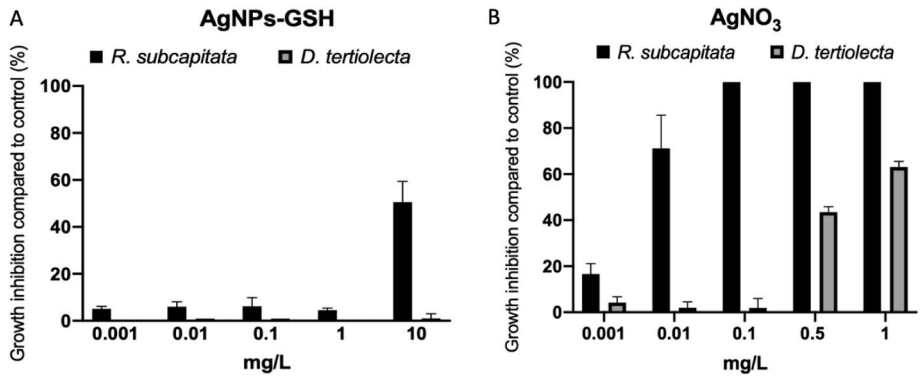

Fig. 7. Growth inhibition compared to control of *R. subcapitata* (black) and *D. tertiolecta* (gray) exposed to AgNPs-cit-GSH (**a**) and $AgNO_3$ (**b**) for 72 h. Data are expressed as mean ± SD.

CRediT authorship contribution statement

Arianna Bellingeri: Methodology, Data curation, Investigation. **Federica Bertelà:** Methodology, Data curation, Investigation. **Luca Burratti:** Methodology, Investigation, Data Curation, Writing. **Andrea Calantropio:** Investigation, Data Curation. **Chiara Battocchio:** Conceptualization, Formal analysis. **Pietro Lupetti:** Investigation, Data Curation. **Eugenio Paccagnini:** Investigation, Data Curation. **Giovanna Iucci:** Investigation, Data Curation. **Martina Marsotto:** Investigation, Data Curation. **Paolo Prosposito:** Conceptualization, Data curation. **Ilaria Corsi:** Conceptualization, Data curation. **Iole Venditti:** Conceptualization, Methodology, Data curation, Investigation, Resources, Writing – original draft, Writing – review & editing.

Declaration of competing interest

The authors declare that they have no known competing financial interests or personal relationships that could have appeared to influence the work reported in this paper.

Data availability

No data was used for the research described in the article.

Acknowledgments

The Grant of Excellence Departments 2023–2027, MIUR (ARTICOLO 1, COMMI 314–337 LEGGE 232/2016), and Rome Technopole Project (CUP:F83B22000040006) are gratefully acknowledged by authors of Roma Tre University. HR-XPS measurements were carried out at the PM4/LowDosePES instrument at the BESSY II electron storage ring operated by the Helmholtz-Zentrum Berlin für Materialien und Energie; authors from Roma Tre University gratefully thank Dr. E. Giangrisostomi for assistance during the experiment. This research was partially funded by FESR Fondo Europeo di Sviluppo Regionale – Programma Operativo regionale del Lazio, Programmazione 2014–2020, Progetti Gruppi di Ricerca 2020 – protocollo GeCoWEB n. A0375-2020-36521, CUP E85F21002440002.

Appendix A. Supplementary data

Supplementary data to this article can be found online at https://doi.org/10.1016/j.matchemphys.2023.128671.

References

[1] J.S. Manser, J.A. Christians, P.V. Kamat, Intriguing optoelectronic properties of metal halide perovskites, Chem. Rev. 116 (2016) 12956–13008, https://doi.org/10.1021/acs.chemrev.6b00136.

[2] Q.H. Wang, K. Kalantar-Zadeh, A. Kis, J.N. Coleman, M.S. Strano, Electronics and optoelectronics of two-dimensional transition metal dichalcogenides, Nat. Nanotechnol. 7 (2012) 699–712, https://doi.org/10.1038/nnano.2012.193.

[3] G. Naponiello, I. Venditti, V. Zardetto, D. Saccone, A. Di Carlo, I. Fratoddi, C. Barolo, D. Dini, Photoelectrochemical characterization of squaraine-sensitized nickel oxide cathodes deposited via screen-printing for p-type dye-sensitized solar cells, Appl. Surf. Sci. 356 (2015) 911–920, https://doi.org/10.1016/j.apsusc.2015.08.171.

[4] K. Jomova, M. Makova, S.Y. Alomar, S.H. Alwasel, E. Nepovimova, K. Kuca, C. J. Rhodes, M. Valko, Essential metals in health and disease, Chem. Biol. Interact. 367 (2022), 110173, https://doi.org/10.1016/j.cbi.2022.110173.

[5] I. Kostova, The role of complexes of biogenic metals in living organisms, INORGA 11 (2023) 56, https://doi.org/10.3390/inorganics11020056.

[6] L. Burratti, E. Bolli, M. Casalboni, F. De Matteis, F. Mochi, R. Francini, S. Casciardi, P. Prosposito, Synthesis of fluorescent ag nanoclusters for sensing and imaging applications, Mater. Sci. Forum 941 (2018) 2243. https://doi.org/10.4028/www.scientific.net/MSF.941.2243.

[7] C.D. Lewis, U.K. Laemmli, Higher-order metaphase chromosome structure – evidence for metalloprotein interactions, Cell 29 (1982) 171–181, https://doi.org/10.1016/0092-8674(82)90101-5.

[8] G.-P. Tao, Q.-Y. Chen, X. Yang, K.-D. Zhao, J. Gao, Targeting cancer cells through iron(III) complexes of di(picolyl)amine modified silica core–shell nanospheres, Colloids Surf., B 86 (2011) 106–110, https://doi.org/10.1016/j.colsurfb.2011.03.026.

[9] L. Wang, Y.-L. Yin, X.-Z. Liu, P. Shen, Y.-G. Zheng, X.-R. Lan, C.-B. Lu, J.-Z. Wang, Current understanding of metal ions in the pathogenesis of Alzheimer's disease, Transl. Neurodegener. 9 (2020) 10, https://doi.org/10.1186/s40035-020-00189-z.

[10] D.L. Rocha, V. Maringolo, A.N. Araújo, C.M.P.G. Amorim, M. da Conceição, B.S. M. Montenegro, An overview of structured biosensors for metal ions determination, Chemosensors 9 (2011) 324, https://doi.org/10.3390/chemosensors9110324.

[11] D.C. Crans, K. Kostenkova, Open questions on the biological roles of first-row transition metals, Commun. Chem. 3 (2020) 104, https://doi.org/10.1038/s42004-020-00341-w.

[12] K. Ferrao, N. Ali, K.J. Mehta, Iron and iron-related proteins in alcohol consumers: cellular and clinical aspects, J. Mol. Med. 100 (2022) 1673–1689, https://doi.org/10.1007/s00109-022-02254-8.

[13] A. Kappler, C. Bryce, M. Mansor, U. Lueder, J. M Byrne, E. D Swanner, An evolving view on biogeochemical cycling of iron, Nat. Rev. Microbiol. 19 (2021), https://doi.org/10.1038/s41579-020-00502-7.

[14] P.W. Boyd, M.J. Ellwood, The biogeochemical cycle of iron in the ocean, Nat. Geosci. 3 (2010) 675–682, https://doi.org/10.1038/ngeo964.

[15] J. Paluch, P. Kościelniak, I. Molęda, K. Machowski, S. Kalinowski, S. Koronkiewicz, J. Kozak, Novel approach to determination of Fe(II) using a flow system with direct-injection detector, Monatsh. Chem. 151 (2020) 1305–1310, https://doi.org/10.1007/s00706-020-02649-8.

[16] P. Song, L. Zhang, H. Long, M. Meng, T. Liu, Y. Yin, R. Xi, A multianalyte fluorescent carbon dots sensing system constructed based on specific recognition of Fe(III) ions, RSC Adv. 7 (2017) 28637–28646, https://doi.org/10.1039/C7RA04122E.

[17] H. Ye, Y. Liu, W. Xie, X. Lin, H. Pan, Ag nanoparticles/PbTiO3 with in-situ photocatalytic process and its application in an ultra-sensitive molecularly imprinted hemoglobin detection, Collolids Surf. B. 217 (2022), 112641, https://doi.org/10.1016/j.colsurfb.2022.112641.

[18] K. Ghosh, S. Rathi, R. Kushwaha, Sensing of Fe(III) ion via turn-on fluorescence by fluorescence probes derived from 1-naphthylamine, Tetrahedron Lett. 54 (2013) 6460–6463, https://doi.org/10.1016/j.tetlet.2013.09.066.

[19] J. Li, Q. Wang, Z. Guo, H. Ma, Y. Zhang, B. Wang, D. Bin, Q. Wei, Highly selective fluorescent chemosensor for detection of Fe3+ based on Fe3O4@ZnO, Sci. Rep. 6 (6) (2016), 23558, https://doi.org/10.1038/srep23558.

[20] I. Schiesaro, C. Battocchio, I. Venditti, P. Prosposito, L. Burratti, P. Centomo, C. Meneghini, Structural characterization of 3d metal adsorbed AgNPs, Phys. E

Low-dimens. Syst. Nanostruct. 123 (2020), 114162, https://doi.org/10.1016/j.physe.2020.114162.
[21] Q. Ma, J. Song, S. Zhang, M. Wang, Y. Guo, C. Dong, Selective colorimetric and fluorimertic sensor of Hg (II) ion from silver nanoparticles using Acacia chundra leaves extract, Mater. Chem. Phys. 287 (2022), 126284, https://doi.org/10.1016/j.matchemphys.2022.126284.
[22] E. Bolli, A. Mezzi, L. Burratti, P. prosposito, S. Casciardi, S. Kaciulis, X-ray and UV photoelectron spectroscopy of Ag nanoclusters, Surf. Interface Anal. 52 (2020) 1017–1022, https://doi.org/10.1002/sia.6783.
[23] Y. Yao, D. Tian, H. Li, Cooperative binding of bifunctionalized and click-synthesized silver nanoparticles for colorimetric Co2+ sensing, ACS Appl. Mater. Interfaces 2 (3) (2010) 684–690, https://doi.org/10.1021/am900741h.
[24] M. Iannelli, A. Bellini, I. Venditti, B. Casentini, C. Battocchio, M. Scalici, S. Ceschin, Differential phytotoxic effect between silver nitrate (AgNO3) and bifunctionalized silver nanoparticles (AgNPs-cit-L-Cys) on Lemna plants (duckweeds), Aquat. Toxicol. 250 (2022), 106260, https://doi.org/10.1016/j.aquatox.2022.106260.
[25] R.P. Modi, V.N. Mehta, S.K. Kailasa, Bifunctionalization of silver nanoparticles with 6 mercaptonicotinic acid and melamine for simultaneous colorimetric sensing of Cr3+ and Ba2+ ions, Sensor. Actuator. B Chem. 195 (2014) 562–571, https://doi.org/10.1016/j.snb.2014.01.059.
[26] J. Du, J. Tang, S. Xu, J. Ge, Y. Dong, H. Li, M. Jin, A review on silver nanoparticles-induced ecotoxicity and the underlying toxicity mechanisms, Regul. Toxicol. Pharmacol. 98 (2018) 231–239, https://doi.org/10.1016/j.yrtph.2018.08.003.
[27] I. Corsi, I. Venditti, F. Trotta, C. Punta, Environmental safety of nanotechnologies: the eco-design of manufactured nanomaterials for environmental remediation, Sci. Total Environ. 864 (2023), 161181, https://doi.org/10.1016/j.scitotenv.2022.161181.
[28] S. Kheiri, X. Liu, M. Thompson, Nanoparticles at biointerfaces: antibacterial activity and nanotoxicology, Colloids Surf., B 184 (2019), 110550, https://doi.org/10.1016/j.colsurfb.2019.110550.
[29] P. Prosposito, L. Burratti, A. Bellingeri, G. Protano, C. Faleri, I. Corsi, C. Battocchio, G. Iucci, L. Tortora, V. Secchi, S. Franchi, I. Venditti, Bifunctionalized silver nanoparticles as Hg2+ plasmonic sensor in water: synthesis, characterizations and ecosafety, Nanomaterials 9 (2019) 1353, https://doi.org/10.3390/nano9101353.
[30] A. Bellingeri, M. Scattoni, I. Venditti, C. Battocchio, G. Protano, I. Corsi, Ecologically based methods for promoting safer nanosilver for environmental applications, J. Hazard Mater. 438 (2022), 129523, https://doi.org/10.1016/j.jhazmat.2022.129523.
[31] E. Tomaszewska, K. Soliwoda, K. Kadziola, B. Tkacz-Szczesna, G. Celichowski, M. Cichomski, W. Szmaja, J. Grobelny, Detection limits of DLS and UV-vis spectroscopy in characterization of polydisperse nanoparticles colloids, J. Nanomater. 2013 (2013), 313081, https://doi.org/10.1155/2013/313081.
[32] I. Venditti, A. Cartoni, S. Cerra, R. Fioravanti, T.A. Salamone, F. Sciubba, M. A. Tabocchini, V. Dini, C. Battocchio, G. Iucci, L. Carlini, R. Faccini, F. Collamati, C. Mancini Terracciano, E. Solfaroli Camillocci, S. Morganti, A. Giordano, T. Scotognella, D. Maccora, D. Rotili, C. Marchese, E. Anastasiadou, P. Trivedi, I. Fratoddi, Hydrophilic gold nanoparticles as anti-PD-L1 antibody carriers: synthesis and interface properties, part. Part, Syst. Charact. 39 (2022), 2100282, https://doi.org/10.1002/ppsc.202100282.
[33] I. Fratoddi, I. Venditti, C. Cametti, C. Palocci, L. Chronopoulou, M. Marino, F. Acconcia, M.V. Russo, Functional polymeric nanoparticles for dexamethasone loading and release, Colloids Surf., B 93 (2012) 59–66, https://doi.org/10.1016/j.colsurfb.2011.12.008.
[34] J.F. Moulder, W.F. Stickle, P.E. Sobol, K.D. Bomben, Handbook of X-Ray Photoelectron Spectroscopy, Eden Prairie, 1992.
[35] P. Swift, D. Shuttleworth, M.P. Seah, in: D. Briggs, M.P. Seah (Eds.), Practical Surface Analysis by Auger and X-Ray Photoelectron Spectroscopy, J. Wiley & Sons, Chichester, 1983 (chapter 5) appendix 3.
[36] E. Giangrisostomi, R. Ovsyannikov, F. Sorgenfrei, LowDosePES: the low-dose photoelectron spectroscopy end-station at the PM4 beamline at BESSY II, JLSRF 4 (2018) A130, https://doi.org/10.17815/jlsrf-4-114.
[37] I. Fratoddi, C. Battocchio, A. Cartoni, G. Iucci A. Paladini, D. Catone, P. O'Keeffe, S. Nappini, S. Cerra, I. Venditti, Silver nanoparticles functionalized by Rhodamine B isothiocyanate or Fluorescein isothiocyanate: synthesis and studies on fluorescent and plasmonic properties, Appl. Sci. 11 (2021) 2472, https://doi.org/10.3390/app11062472.
[38] X. Gao, Y. Lu, S. He, X. Li, W. Chen, Colorimetric detection of iron ions (III) based on the highly sensitive plasmonic response of the N-acetyl-L-cysteine-stabilized silver nanoparticles, Anal. Chim. Acta 879 (2015) 118–125, https://doi.org/10.1016/j.aca.2015.04.002.
[39] R. Rajamanikandan, M. Ilanchelian, Simple and visual approach for highly selective biosensing of vitamin B1 based on glutathione coated silver nanoparticles as a colorimetric probe, Sensor. Actuator. B Chem. 244 (2017) 380–386, https://doi.org/10.1016/j.snb.2016.12.129.
[40] M. Potara, A.-M. Gabudean, S. Astilean, Solution-phase, dual LSPR-SERS plasmonic sensors of high sensitivity and stability based on chitosan-coated anisotropic silver nanoparticles, J. Mater. Chem. 21 (2011) 3625–3633, https://doi.org/10.1039/C0JM03329D.
[41] G. Roger, B. Pinching, G.D. Pinching, Resolution of the dissociation constants of citric acid at 0 to 50°, and determination of certain related thermodynamic functions, J. Am. Chem. Soc. 71 (1949) 1274–1283, https://doi.org/10.1021/ja01172a039.
[42] D.L. Rabenstein, Nuclear magnetic resonance studies of the acid-base chemistry of amino acids and peptides. I. Microscopic ionization constants of glutathione and methylmercury-complexed glutathione, J. Am. Chem. Soc. 95 (1973) 2797–2803, https://doi.org/10.1021/ja00790a009.
[43] S.P. Wu, Y.P. Chen, Y.M. Sung, Colorimetric detection of Fe3+ ions using pyrophosphate functionalized gold nanoparticles, Analyst 136 (2011) 1887–1891, https://doi.org/10.1039/C1AN15028F.
[44] H.B. Xu, S.H. Zhou, L.L. Xiao, H.H. Wang, S.Z. Li, Q.H. Yuan, Fabrication of a nitrogen-doped graphene quantum dot from MOF-derived porous carbon and its application for highly selective fluorescence detection of Fe3+, J. Mater. Chem. C 3 (2015) 291–297, https://doi.org/10.1039/C4TC01991A.
[45] C.X. Yang, H.B. Ren, X.P. Yan, Fluorescent metal organic framework MIL-53(Al) for highly selective and sensitive detection of Fe3+ in aqueous solution, Anal. Chem. 85 (2013) 7441–7446, https://doi.org/10.1021/ac401387z.
[46] H. Kim, B. Koo, Iron(III) sensors based on the fluorescence quenching of poly (phenylene ethynylene)s and iron-detecting PDMS pads, Macromol. Res. 29 (2021) 360–364, https://doi.org/10.1007/s13233-021-9041-4.
[47] X. Gao, Y. Lu, S. He, X. Li, W. Chen, Colorimetric detection of iron ions (III) based on the highly sensitive plasmonic response of the N-acetyl-l-cysteine-stabilized silver nanoparticles, Anal. Chim. Acta 879 (2015) 118–125, https://doi.org/10.1016/j.aca.2015.04.002.
[48] N.I.S.T. X-ray, Photoelectron Spectroscopy Database, National Institute of Standards and Technology, Gaithersburg, 2012, https://doi.org/10.18434/T4T88K. Version 4.1.
[49] L. Carlini, C. Fasolato, P. Postorino, I. Fratoddi, I. Venditti, G. Testa, C. Battocchio, Comparison between silver and gold nanoparticles stabilized with negatively charged hydrophilic thiols: SR-XPS and SERS as probes for structural differences and similarities, Colloids Surf., A 532 (2017) 183–188, https://doi.org/10.1016/j.colsurfa.2017.05.045.
[50] M.Y. Hamed, J. Silver, Studies on the reactions of ferric iron with glutathione and some related thiols. Part II. Complex formation in the pH range three to seven, Inorg. Chim. Acta. 80 (1983) 115–122, https://doi.org/10.1016/S0020-1693(00)91271-4.
[51] F. Bertelà, M. Marsotto, C. Meneghini, L. Burratti, M. Valentin-Adrian, G. Iucci, I. Venditti, P. Prosposito, V. D'Ezio, T. Persichini, C. Battocchio, Biocompatible silver nanoparticles: study of the chemical and molecular structure, interaction to cadmium and arsenic in water and biological properties, Nanomaterials 11 (2021) 2540, https://doi.org/10.3390/nano11102540.
[52] I. Pedre, F. Battaglini, G.J. Labrada Delgado, M.G. Sánchez-Loredo, G.A. González, Detection of thiourea from electrorefining baths using silver nanoparticles-based sensors, Sensor. Actuator. B Chem. 211 (2015) 515–522, https://doi.org/10.1016/j.snb.2015.01.074.
[53] I. Pedre, G.A. Gonzalez, Silver nanoparticles-based sensing platform for Fe3+ ions in complex matrices, Miner. Eng. 185 (2022), 107712, https://doi.org/10.1016/j.mineng.2022.107712.
[54] R.M. Silverstein, G.C. Bassler, T.C. Morrill, Spectrometric Identification of Organic Compounds, Wiley, Chichester, 1991.
[55] M. Kleiven, A. Macken, D.H. Oughton, Growth inhibition in Raphidocelis subcapita–Evidence of nanospecific toxicity of silver nanoparticles, Chemosphere 221 (2019) 785–792, https://doi.org/10.1016/j.chemosphere.2019.01.055.
[56] R. Biba, K. Košpić, B. Komazec, D. Markulin, P. Cvjetko, D. Pavoković, P. Peharec Štefanić, M. Tkalec, B. Balen, Surface coating-modulated phytotoxic responses of silver nanoparticles in plants and freshwater green algae, Nanomaterials 12 (2022) 2, https://doi.org/10.3390/nano12010024.
[57] S.A. Johari, M. Sarkheil, M.B. Tayemeh, S. Veisi, Influence of salinity on the toxicity of silver nanoparticles (AgNPs) and silver nitrate (AgNO3) in halophilic microalgae, Dunaliella salina, Chemosphere 209 (2018) 156–162, https://doi.org/10.1016/j.chemosphere.2018.06.098.
[58] S. Lekamge, A.F. Miranda, A. Abraham, A.S. Ball, R. Shukla, D. Nugegoda, The toxicity of coated silver nanoparticles to the alga Raphidocelis subcapitata, SN Appl. Sci. 2 (2020) 596, https://doi.org/10.1007/s42452-020-2430-z.
[59] C. Levard, B.C. Reinsch, F.M. Michel, C. Oumahi, G.V. Lowry, G.E. Brown Jr., Sulfidation processes of PVP-coated silver nanoparticles in aqueous solution: impact on dissolution rate, Environ. Sci. Technol. 45 (2011) 5260–5266, https://doi.org/10.1021/es2007758.
[60] C. Levard, E.M. Hotze, G.V. Lowry, G.E. Brown Jr., Environmental transformations of silver nanoparticles: impact on stability and toxicity, Environ. Sci. Technol. 46 (2012) 6900–6914, https://doi.org/10.1021/es403527n.
[61] C. Levard, E.M. Hotze, B.P. Colman, A.L. Dale, L. Truong, X. Yang, A.J. Bone, G. E. Brown Jr., R.L. Tanguay, R.T. Di Giulio, Sulfidation of silver nanoparticles: natural antidote to their toxicity, Environ. Sci. Technol. 47 (2013) 13440–13448, https://doi.org/10.1021/es2037405.
[62] B. Pem, I.M. Pongrac, L. Ulm, I. Pavičić, V. Vrček, D.D. Jurašin, M. Ljubojević, A. Krivohlavek, I.V. Vrček, Toxicity and safety study of silver and gold nanoparticles functionalized with cysteine and glutathione, Beilstein J. Nanotechnol. 10 (2019) 1802–1817, https://doi.org/10.3762/bjnano.10.175.
[63] J. Mertens, K. Oorts, D. Leverett, K. Arijs, Effects of silver nitrate are a conservative estimate for the effects of silver nanoparticles on algae growth and Daphnia magna reproduction, Environ. Toxicol. Chem. 38 (2019) 1701–1713, https://doi.org/10.1002/etc.4463.
[64] R.A.D. Lish, S.A. Johari, M. Sarkheil, I.J. Yu, On how environmental and experimental conditions affect the results of aquatic nanotoxicology on brine shrimp (Artemia salina): a case of silver nanoparticles toxicity, Environ. Pollut. 255 (2019), 113358, https://doi.org/10.1016/j.envpol.2019.113358.
[65] C.M. Levard, S. Mitra, T. Yang, A.D. Jew, A.R. Badireddy, G.V. Lowry, G. E. Brown Jr., Effect of chloride on the dissolution rate of silver nanoparticles and toxicity to E. coli, Environ. Sci. Technol. 47 (2013) 5738–5745, https://doi.org/10.1021/es400396f.